Probability distributions of local Lyapunov exponents for Hamiltonian systems

Concezione Amitrano and R. Stephen Berry

The James Franck Institute and Department of Chemistry, The University of Chicago, 5735 South Ellis Avenue, Chicago, Illinois 60637
(Received 13 October 1992)

We calculate the probability distributions of the largest local Lyapunov exponent for three Hamiltonian systems at different values of the energy E, for a set of increasing values of the length in which the trajectory is partitioned. The systems we study are the Hénon-Heiles model and the classical Ar_3 and Ar_7 clusters. We show that these distributions contain much information about the dynamics of the system and, in particular, can be used to study the evolution of ergodic properties as the internal energy of the system increases; therefore, even though the inequivalence of chaos and ergodicity does not allow one to consider Lyaponov exponents to be a direct measure of ergodicity, the sample distributions of short-term Lyapunov exponents can be used to evaluate the extent of ergodic behavior in the various situations.

I. INTRODUCTION

The spectrum of Lyapunov exponents [1-3] has proven to be one of the most useful diagnostics to detect and quantify chaos (for a general review see Ref. [4]). Positive (or negative) Lyapunov exponents measure the asymptotic average exponential (powers of 2) rate of divergence (or convergence) of nearby orbits in phase space and are by definition "global" quantities in time. Exponential divergence implies that predictive power regarding trajectories shows extreme sensitivity to the level of initial information; hence any system with at least one positive Lyapunov exponent is said to be chaotic.

The concept of "local" Lyapunov exponents was examined [5], set aside for a time, and then came of interest again recently [6-8]. In this approach the exponential rate of divergence is averaged only over short stretches of time. Of course, then the results on any two distinct stretches can be different, but it turns out that the distributions of such results are in fact invariants of the dynamical system. For strange attractors these distributions tell about the variation of predictability over the attractor [7]. For Hamiltonian systems it has been suggested that they could be used to separate the power spectra into a regular part exhibiting very sharp peaks, generated by the motion in the vicinity of invariant tori where the divergence of nearby orbits is algebraic (i.e., the largest Lyapunov exponent is zero), and a chaotic background consisting of broadened features, generated by the motion in the regions where the divergence is predominantly exponential [6]. The concept was also used to demonstrate [8] the nonmonotonic energy dependence of the Lyapunov exponents, K entropy, and fractal dimension of trajectories of the Ar_3 cluster [9] in terms of the geometry of the underlying potential surface.

Intrigued by these results, we decided to take up the analysis of conservative systems more complicated than the standard map considered in Ref. [6]; in Ref. [10] we gave some results for the classical Ar_3 cluster [8,9,11,12]. In this paper we examine the probability distributions of

the largest local Lyapunov exponent for the Hénon-Heiles Hamiltonian [13], and for a larger Lennard-Jones classical cluster Ar_7 as a function of the total energy of the system under consideration. In addition we present more details about our calculations for Ar_3. To get the distributions at a given energy we partition the trajectory in phase space into intervals of equal length and calculate the largest Lyapunov exponent separately for each interval; we repeat this process for a set of increasing values of the length of the intervals.

We find that in general the situation is not quite as simple as in Ref. [6], and if indeed one has to distinguish between regions of regular motion and regions of chaos, it is because they generate qualitatively different kinds of distributions: only in the limit of "global high chaos" do both kinds of regions cooperate to produce multifeatured distributions for which it is meaningful to attempt the separation of the power spectrum into spikes and broad background. But the fact that regular regions can be associated with distributions with very clear properties defines in itself a way to distinguish these regions from the chaotic ones. Moreover these distributions quite clearly show the evolution of ergodic behavior with increasing energy, and at fixed energy allow one to identify distinctive, separable time scales for different extents of ergodic behavior. In fact for a realistic system such as the Ar_3 or the Ar_7 cluster they give illuminating information about the dynamics; in particular for Ar_7, a system with more than one stable equilibrium structure [12], they immediately show the relative importance of the various potential minima, and the time scale for the transitions between them.

The paper is organized as follows. In Sec. II we give some technical details on the computational method, introducing the Hamiltonians for our systems and the algorithms used to generate the trajectories and to calculate the Lyapunov exponents. In Sec. III we present our results for the three systems we have studied, showing how the qualitative features of the distributions vary with the energy of the system. To extract the properties of the

distributions we analyze their scaling behavior as a function of the length of the partitioning interval, and we also study the time autocorrelation function of the local Lyapunov exponents. Moreover, we show that for Ar_3 and Ar_7 the correlation between short-term Lyapunov exponents and short-term average kinetic energy yields plots which can be used as tools to understand the dynamics. One can then perform a power spectrum analysis analogous to that presented in Ref. [6]. Finally, Sec. IV contains a discussion that concludes the paper.

II. COMPUTATIONAL METHOD

Hénon and Heiles introduced the Hamiltonian named after them in the context of astronomical dynamics [13]. In our context, its most straightforward interpretation is that of a system with the two stretching vibrational degrees of freedom of a linear triatomic molecule with periodic boundary conditions [14]:

$$H = \tfrac{1}{2}(p_x^2 + p_y^2) + \tfrac{1}{2}(x^2 + y^2 + 2x^2 y - \tfrac{2}{3}y^3) \ . \tag{1}$$

The potential is binding for $E \leq \tfrac{1}{6}$; the equipotential at $E = \tfrac{1}{6}$ is the equilateral triangle $x = \pm(y-1)/\sqrt{3}$, $y = -\tfrac{1}{2}$. The Poincaré surface of section for energies $\leq \tfrac{1}{12}$ shows smooth lines [Fig. 1(a)], representative of the fact that the system is close to integrable, and the thin layers of stochasticity associated with the resonances between the degrees of freedom, though densely distributed through the entire surface of section, occupy only a negligible fraction of the total area [15]. For energies $\simeq \tfrac{1}{8}$ we can see three kinds of orbits [Fig. 1(b)]: simple invariant curves like the ones found before, multiple-loop curves, and apparently ergodic orbits. At energies $\simeq \tfrac{1}{6}$, except for the persistence of a few regular curves, almost all the surface area is occupied by chaotically distributed intersections [Fig. 1(c)].

To describe the classical Ar_3 and Ar_7 clusters we take the Lennard-Jones Hamiltonian

$$H = \sum_{i=1}^{n} \frac{p_i^2}{2m} + 4\varepsilon \sum_{\substack{i,j=1 \\ (i<j)}}^{n} \left[\left[\frac{\sigma}{r_{ij}} \right]^{12} - \left[\frac{\sigma}{r_{ij}} \right]^6 \right] \ , \tag{2}$$

where $n = 3$ for Ar_3 and $n = 7$ for Ar_7, p_i are the linear momenta for the atoms, r_{ij} are the interatomic distances, and the parameters m, σ, and ε are chosen to match the experimentally obtained values for argon, namely, $m = 39.45$ amu, $\sigma = 3.4$ Å, and $\varepsilon = 1.67 \times 10^{-14}$ ergs.

The trajectories are generated by using the following molecular-dynamics algorithm:

$$q_i(t_n) = q_i(t_{n-1}) + \frac{\tau}{m} p_i(t_{n-1}) + \frac{\tau^2}{2m} \frac{\partial V}{\partial q_i}(t_{n-1}) \ , \tag{3a}$$

$$p_i(t_n) = p_i(t_{n-1}) + \frac{\tau}{2m} \left[\frac{\partial V}{\partial q_i}(t_n) + \frac{\partial V}{\partial q_i}(t_{n-1}) \right] \tag{3b}$$

(the velocity version of the Verlet algorithm [16,17]). In Eqs. (3) q_i are the coordinates, p_i are the momenta, V is the potential, m is the mass, and τ is the time step; the latter should be chosen small enough to conserve the to-

tal energy of the system during the simulation, and we took $\tau = 0.01$ for the Hénon-Heiles integration and $\tau = 10^{-14}$ s for the argon clusters integrations (this choice makes one vibrational period of argon correspond to 100–150 steps). For the argon clusters we chose the initial conditions so that the center of mass and the total angular momentum are zero, and they remain constant dur-
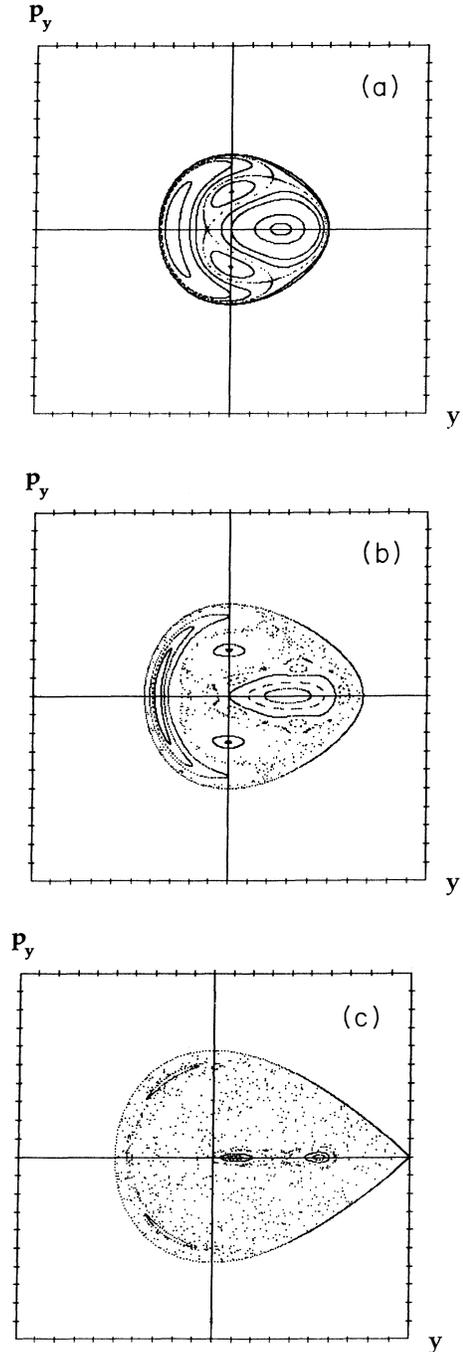
FIG. 1. Surfaces of Poincaré section $x = 0$ for the Hénon-Heiles potential at (a) $E = \tfrac{1}{12}$, (b) $E = \tfrac{1}{8}$, and (c) $E = \tfrac{1}{6}$. Both of the axes go from -1 to $+1$.

ing the simulation. A temperature T can be defined through the equipartition theorem as the mean vibrational kinetic energy for the run, i.e.,

$$T = \frac{2n\langle E_{kin}\rangle}{(3n-6)k_B} ,$$ (4)

where k_B is the Boltzmann constant, n is the number of atoms, $(3n-6)$ is the number of vibrational degrees of freedom, and $\langle E_{kin}\rangle$ is the kinetic energy averaged over a long trajectory.

As stated, our goal is to obtain and study the distributions of sample values of the largest Lyapunov exponent on various time scales. For a d-dimensional space the local Lyapunov exponents $\lambda_1^{(N)}, \lambda_2^{(N)}, \ldots, \lambda_d^{(N)}$ are calculated by propagating the Jacobian along the trajectory for $N-1$ steps, yielding

$$\{2^{\lambda_1^{(N)}}, 2^{\lambda_2^{(N)}}, \ldots, 2^{\lambda_d^{(N)}}\}$$
$$= \left[\text{magnitude of eigenvalues of} \prod_{n=0}^{N-1} J(\mathbf{x}_n)\right]^{1/N} ,$$ (5)

where $J(\mathbf{x}_n)$ is the Jacobian matrix of the propagators for each phase-space variable [18,4]. Of course the Lyapunov exponents would be found exactly by taking the limit $N \rightarrow \infty$.

The algorithm for computing the Lyapunov exponents involved calculating the Jacobian matrix at each time step, multiplying that matrix by the cumulative product of all the previous ones, and diagonalizing the final product after N time steps. Those eigenvalues are then converted to Lyapunov exponents by taking their logarithm and dividing by N. This method in the long-time limit should be equivalent [19,20] to that of Benettin et al. [3], and has been verified in this work to be so. Notice that even if we are only interested in the largest Lyapunov exponent we still have to calculate all of them to find the maximum, since in a relatively small number of time steps the repeated application of the Jacobian matrix might not have completely succeeded in aligning an arbitrary vector to the direction of the eigenvector corresponding to the largest eigenvalue.

In the present case one is interested in calculating the largest Lyapunov exponent $\lambda^{(N)} = \max_i \{\lambda_i^{(N)}\}$ for a set of increasing values of N. To speed our algorithm by saving matrix multiplications we limit ourselves to the following values of N: $\{2^i\}$, $i = 7,8,9,10,11,12,13$, or $N_i = \{128, 256, \ldots, 8192\}$, since for each of these values the product after N_i time steps can be obtained as the product of two N_{i-1} matrices. Previous tests had demonstrated that our simulations begin to lose mechanical reversibility between 5000 and 10 000 steps, so that our longest averages are still within the range that maintains that reversibility.

For Ar_3 our simulations typically ran for $10^9 - 10^{10}$ time steps (total time of $10^{-5} - 10^{-4}$ s), and started from a small number of different initial conditions that had already equilibrated. The distributions presented in this work contain from $\simeq 10^6$ sample values for trajectories of

length 128 to $\simeq 10^5$ sample values of the Lyapunov exponents for trajectories of length 8192, and no smoothing routine has been applied to them. Much shorter simulations ($\simeq 10^7$) were found to give the same qualitative amount of information, although the actual plots look much rougher and might need smoothing routines. Ar_7 results were obtained by trajectories of $\simeq 10^8$ time steps, while for Hénon-Heiles, for which the trends were more immediately evident, sometimes we stopped after $\simeq 10^7$ time steps; in any case we always show the raw data.

III. RESULTS

A. Hénon-Heiles model

Figure 2 shows four distributions for $E = \frac{1}{12}$, $N = 256$; we plot the quantity $g_{N_i}(\lambda)d\lambda$, i.e, the number of times λ, the largest Lyapunov exponent, was found in a bin of size 2.5×10^{-5} bits per 10^{-2} s versus λ, given in bits per 10^{-2} s, for trajectories of 256 steps, our shortest averaging length. The distributions are normalized in such a way that the area under the curve is 1.

To discuss these results we again refer to Fig. 1: the distributions (a)–(d) are obtained by the trajectories whose Poincaré section is given in the inset and can be compared with the general picture for trajectories of this energy, Fig. 1(a). As we can clearly see the shapes of these distributions are not even remotely Gaussian, as we would expect if the local Lyapunov exponent were also a global quantity with a small uncertainty, but present well-defined features, albeit strongly dependent on the orbit. The shape also depends on the length of the partitioning integral N; to illustrate this point Fig. 3 shows the results for the same orbits as before, but for $N = 1024$: the distributions do not fall one on top of the other, nor do they do so for larger N.

Another interesting feature is illustrated in Fig. 4, where we give the distributions for 256 step averages on two orbits with Poincaré sections in the same class, the "crescent," to be compared with the distribution of Fig. 2(a), also a crescent: the shape of the distribution identifies the type of orbit. But the Poincaré section of Fig. 4(a) is smaller, and the Poincaré section of Fig. 4(b) is larger than our original choice of crescent, Fig. 2(a), and we can observe that although the shapes of these three distributions are very similar the peak distinctly moves to the right as the crescent becomes larger, or on average larger crescents correspond to more chaos than smaller ones. In this sense the distributions c and d of Fig. 2 belong to the same "kidney" class in Fig. 1(a), and their distributions both show three peaks, with b, the larger kidney, presenting more "chaos." At $E = \frac{1}{12}$ the most disordered orbit is d, which can be obtained as the limit in which the crescent shape goes into a complicated self-intersecting curve, and accordingly its distribution has the largest average value of the lot.

What happens now when we raise the energy of the system to, say, $E = \frac{1}{8}$? Let's look at it in the reverse order as before. At this energy the orbit corresponding to d at $E = \frac{1}{12}$ has become chaotic, and the distributions start

looking smoother [Fig. 5(a) for $N=256$]; however, the distributions for the smaller crescents still show peaks [Fig. 5(b)], while the distributions for the larger crescents are intermediate between the ones for regular and the ones for chaotic behavior, with small peaks on a continuous, unimodal background [Fig. 5(c)]. The distributions for a small [Fig. 5(d)] and a large kidney [Fig. 5(e)], and the one for a five island orbit [Fig. 5(f)] present completely resonant behavior.

It is clear now what happens for still higher energies, up to $E=\frac{1}{6}$: the general case will give a smooth curve [Fig. 6(a)], but regular orbits like the one shown in the inset of Fig. 6(b) will still present peaks (both of the distributions of Fig. 6 are for $E=\frac{1}{6}$).

One final remark in this section is that all the distributions shown here have a quite large first bin (the one that corresponds to very small Lyapunov exponents) that cannot be directly plotted in the figures because it falls outside the scale; however, the total area under the curves given is always normalized to 1, and therefore the relative size of the first bin can be indirectly appreciated through its effect on the apparent areas in the figures.

B. Ar₃ cluster

To discuss our results for Ar₃ we are going to need the caloric curve for the system (Fig. 7), i.e., the graph of the temperature as defined in Eq. (4) versus the energy per particle. The curve increases smoothly for a while, then has a kink between the energy of $\simeq -1.15 \times 10^{-14}$ and -0.9×10^{-14} ergs/atom, at a temperature around $\simeq 29$ K, and finally increases again. Ar₃ has one stable geometry, the equilateral triangle: the kink corresponds to the energy where the cluster can "open up" in any of three equivalent ways and then go back to the original configuration; in clusters the passage over the saddle between two potential wells is associated with the "melting" transitions between a solid structure and a floppy shape [9]. Figure 7 roughly divides the energy range in three intervals, below, at, and above the critical temperature.

Let us start by looking at the distributions for the low-energy–low-temperature regime. Figure 8 shows two $N=256$ distributions for $E=1.610 \times 10^{-14}$ ergs/atom, $T=4.15$ K, whose only difference is the initial condition of the argon cluster. Again on the y axis we plot $g_{N_i}(\lambda)d\lambda$ (or the number of times λ was found in a bin of size 2.5×10^{-4} bits per 10^{-14} s for trajectories of length N_i). On the x axis the Lyapunov exponents are given in bits per 10^{-14} s; the area under the curve is normalized to 1.

The distributions differ markedly, and show no tendency to converge over all the time scales we have probed, however long the run is. In fact, substantially they corre-
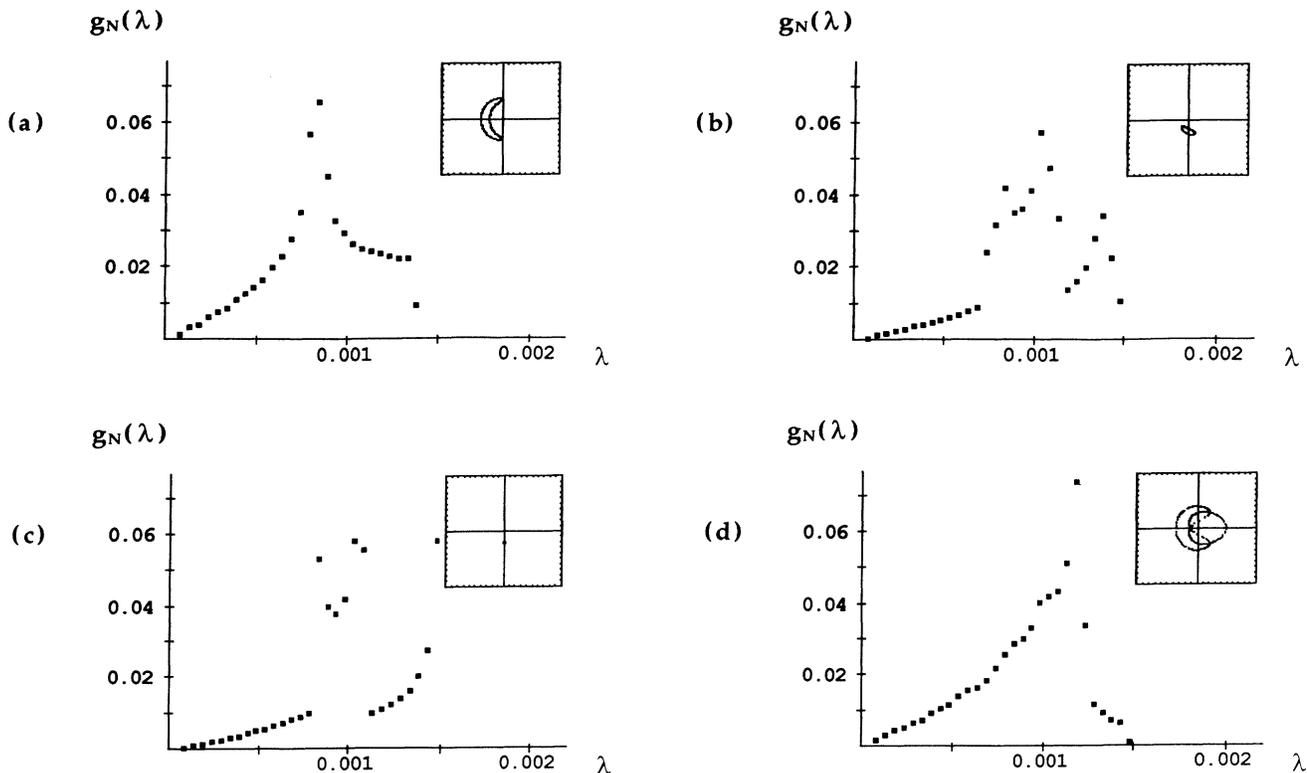
FIG. 2. $g_N(\lambda)$ vs λ at $E=\frac{1}{12}$, $N=256$, for four different initial conditions, with the insets giving the relative Poincaré sections at $x=0$. The units for λ are bits per 10^{-2} s.
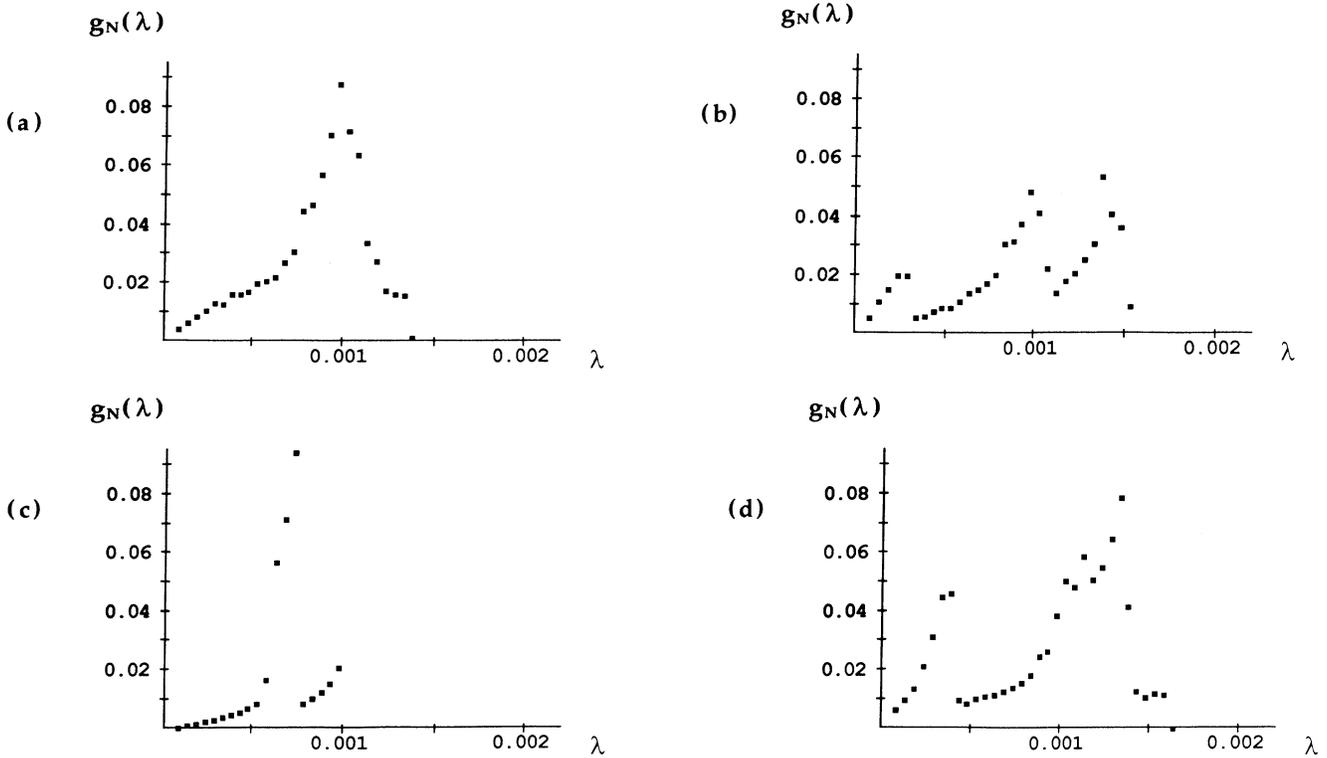
FIG. 3. $g_N(\lambda)$ vs λ at $E = \frac{1}{12}$, $N = 1024$, for the four different initial conditions of Fig. 2. The units for λ are bits per 10^{-2} s.

spond to motions on different torii, and their shapes stay unaltered for what for practical purposes can be considered infinite time *for all lengths of partitioning* N_i. Moreover, the averages and the standard deviations of these distributions depend on the initial conditions for any N_i. Thus we conclude that at this temperature there is total nonergodicity up to at least tens of μs. In this case even averaging over 10^5 time steps will still only give a *local* Lyapunov exponent [21,22].

Of course after looking at the distributions for the

Hénon-Heiles model Fig. 8 does not seem as shocking as it seemed to us in the beginning. In fact as in the Hénon-Heiles case the shape of the distribution can be related to the orbit. Moreover, even more clearly than in the Hénon-Heiles case, we can see that as we increase the energy of the system adiabatically, keeping the shape of the orbit unaltered, the shape of the distribution stays clearly recognizable: Fig. 9 shows the distributions at $E = -1.526 \times 10^{-14}$ ergs/atom, $T = 10.10$ K, of two orbits evolved from the ones to which Fig. 8 refers.
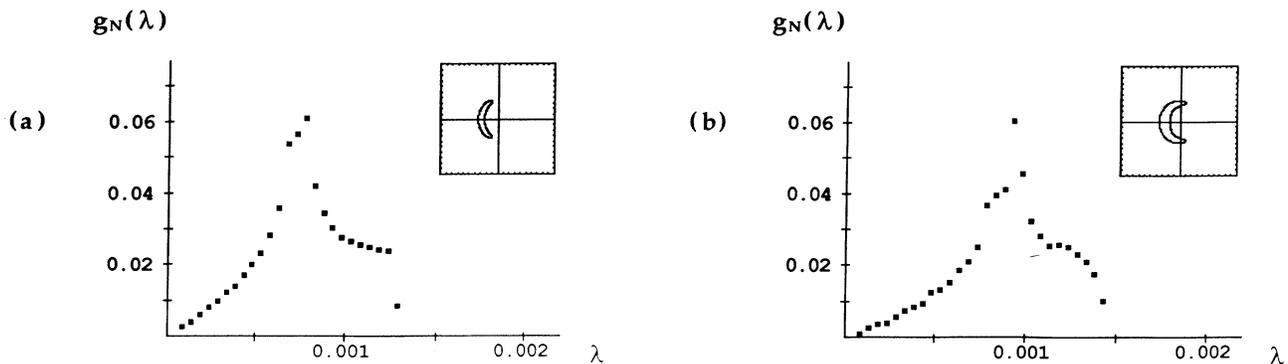
FIG. 4. Two more distributions $g_N(\lambda)$ vs λ at $E = \frac{1}{12}$, $N = 256$, with the insets giving the relative Poincaré sections at $x = 0$. The units for λ are bits per 10^{-2} s.

In fact we observe nonergodicity up to $T \simeq 16$ K: in addition to $E = -1.526 \times 10^{-14}$ ergs/atom we have probed the energies -1.457 and -1.429×10^{-14} ergs/atom, corresponding to the mean temperatures 14.56 and 16.13 K; again, all these distributions, being only finite statistical samples of hypothetical infinite distributions, depend on initial conditions, and in this energy range, very sensitively. However, the higher the temperature, the less the dependence on the initial conditions; at $T = 16.13$ K distributions derived from different initial conditions almost coincide visually, even though

the average and standard deviations of the distributions are still different.

Another way to appreciate the same phenomenon, lack of ergodicity, is to look at the time autocorrelation function of the local largest Lyapunov exponent,

$$\Gamma_N(t) = \frac{\langle (\lambda_N(t) - \langle \lambda_N(t) \rangle)(\lambda_N(0) - \langle \lambda_N(0) \rangle) \rangle}{\langle (\lambda_N(0) - \langle \lambda_N(0) \rangle)^2 \rangle}, \quad (6)$$

over the entire range of energies. A quantity like this quickly goes to zero if there are no long-time correlations
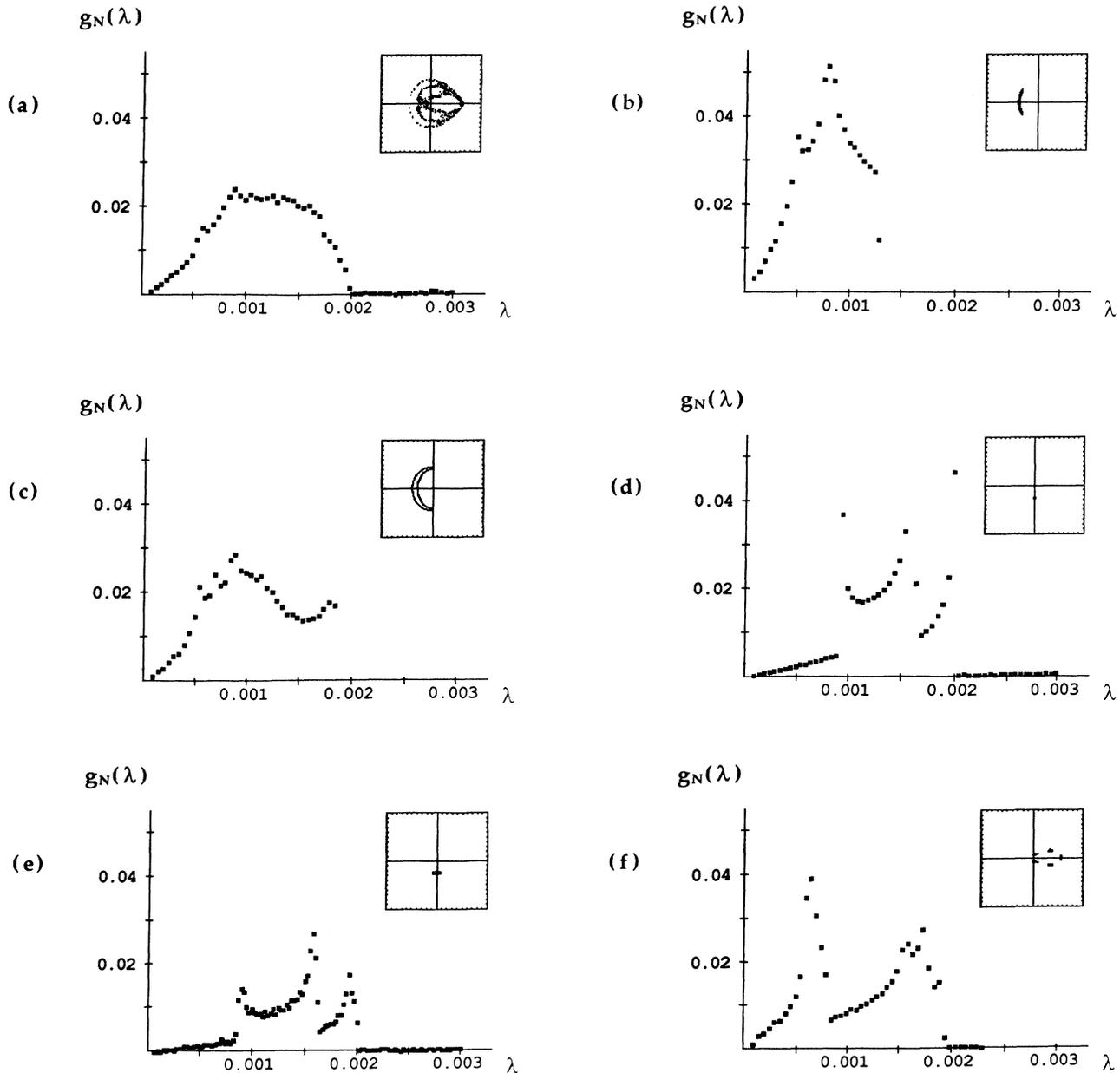
FIG. 5. $g_N(\lambda)$ vs λ at $E = \frac{1}{8}$, $N = 256$, for six different initial conditions, with the insets giving the relative Poincaré sections at $x = 0$. The units for λ are bits per 10^{-2} s.
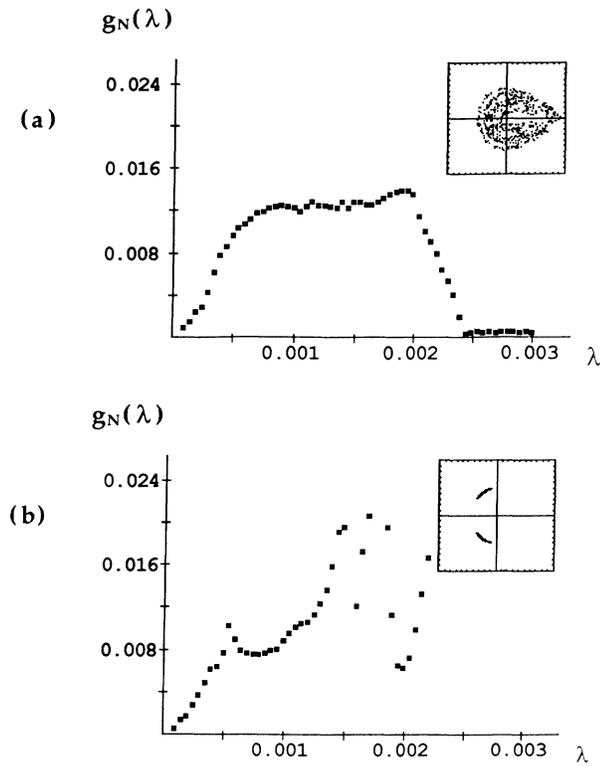
FIG. 6. $g_N(\lambda)$ vs λ at $E = \frac{1}{6}$, $N = 256$, for two different initial conditions, (a) one chaotic, and (b) one regular with their Poincaré sections at $x = 0$. The units for λ are bits per 10^{-2} s.

in the system. Instead, at low temperature $\Gamma_N(t)$ precisely shows long-time correlations, as we can see in Fig. 10(a): a strange periodic pattern, strongly dependent on the initial conditions, appears as the time autocorrelation function at $T = 14.56$ K for the $N = 256$ distribution and a particular but arbitrary choice of the initial conditions.
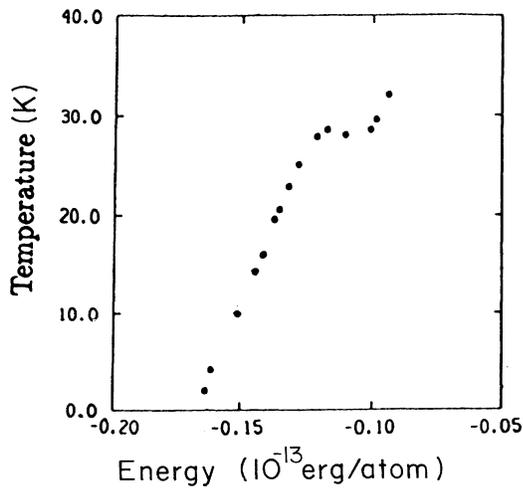
FIG. 7. Caloric curve for Ar_3. The energy is in 10^{-13} ergs per atom and the temperature is in kelvins.
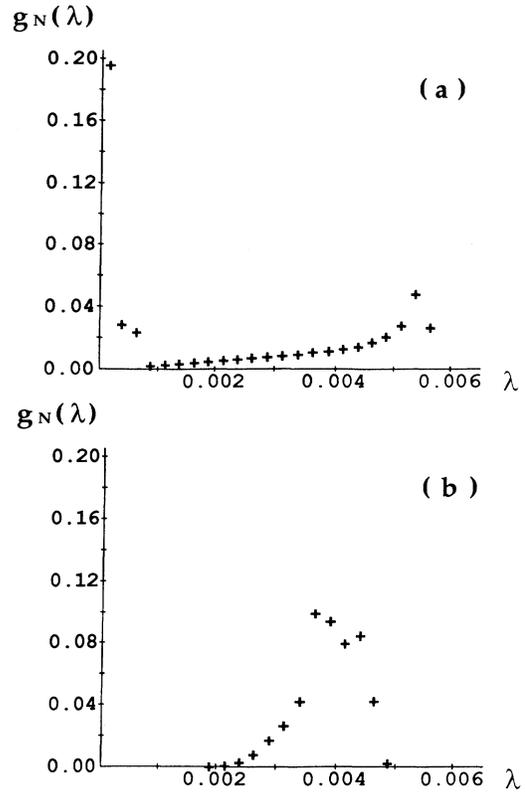
FIG. 8. $g_N(\lambda)$ vs λ at $T = 4.15$ K, $N = 256$, for two different initial conditions of Ar_3. The units for λ are bits per 10^{-14} s.
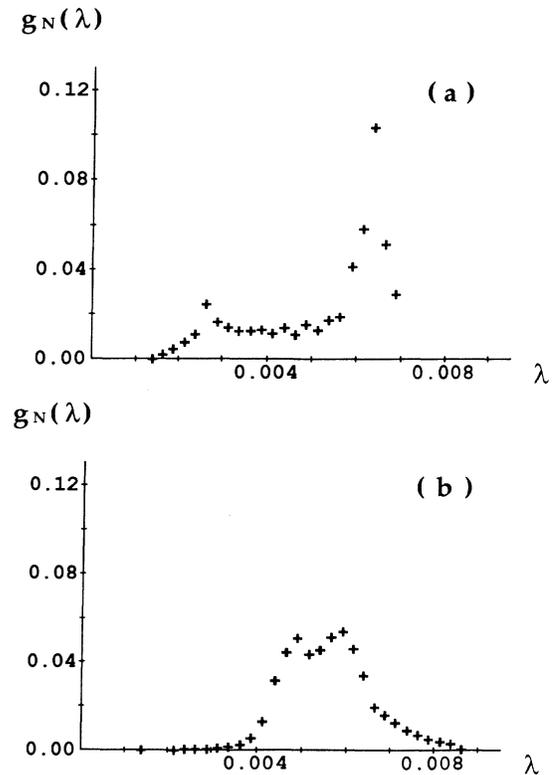
FIG. 9. $g_N(\lambda)$ vs λ at $T = 10.10$ K, $N = 256$, for the two different initial conditions of Ar_3 in Fig. 8. The units for λ are bits per 10^{-14} s.
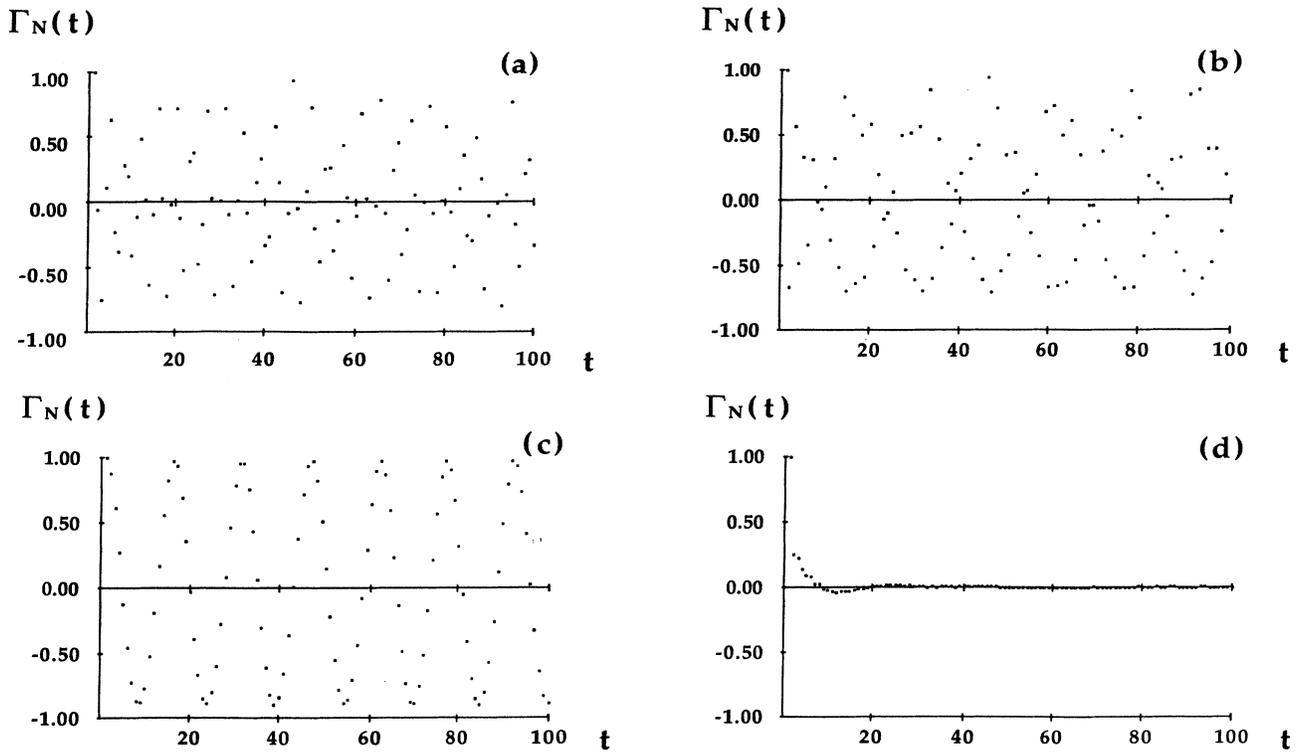
FIG. 10. $\Gamma_N(t)$ [Eq. (6)] at $T=14.56$ K for (a) $N=256$, (b) $N=512$, (c) $N=1024$, and (d) at $T=18.15$ K for $N=256$.
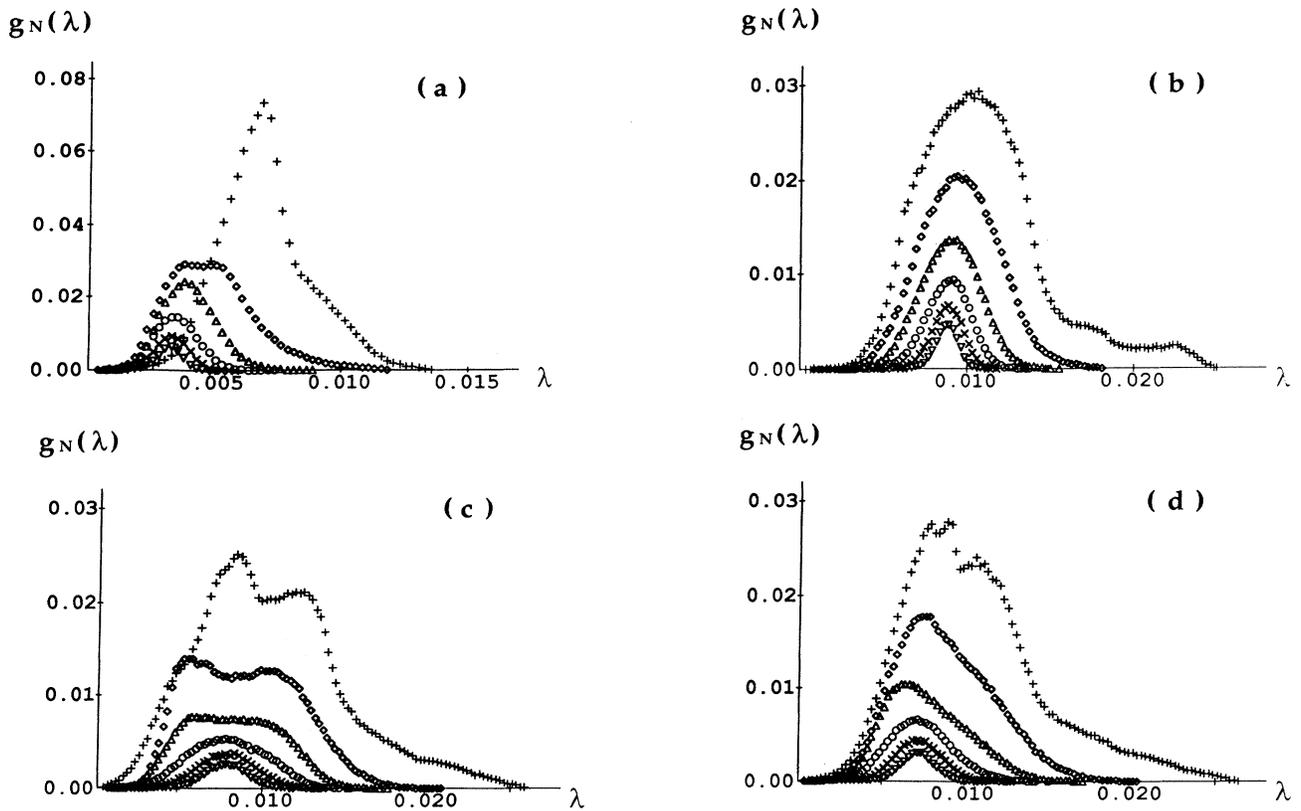
FIG. 11. $g_N(\lambda)$ vs λ at (a) $T=18.15$ K, (b) $T=28.44$ K, (c) $T=30.65$ K, (d) $T=36.71$, K, for $N=256$ (+), $N=512$ ($\Diamond$), $N=1024$ ($\triangle$), $N=2048$ ($\circ$), $N=4096$ ($\times$), and $N=8192$ (∇). The units for λ are bits per 10^{-14} s.

TABLE I. Average value of λ at $T=18.15$ K, 28.44, 30.65, and 36.71 K, for $N=128$, 256, 512, 1024, 2048, 4096, and 8192. The units are bits per 10^{-14} s.

N \ T	18.15	28.44	30.65	36.71
128	1.13×10^{-2}	1.63×10^{-2}	1.47×10^{-2}	1.59×10^{-2}
256	6.98×10^{-3}	1.09×10^{-2}	1.05×10^{-2}	1.05×10^{-2}
512	4.92×10^{-3}	9.58×10^{-3}	8.98×10^{-3}	8.84×10^{-3}
1024	4.08×10^{-3}	9.00×10^{-3}	8.29×10^{-3}	7.76×10^{-3}
2048	3.57×10^{-3}	8.83×10^{-3}	7.98×10^{-3}	7.34×10^{-3}
4096	3.36×10^{-3}	8.78×10^{-3}	7.89×10^{-3}	7.19×10^{-3}
8192	3.28×10^{-3}	8.76×10^{-3}	7.86×10^{-3}	7.14×10^{-3}

For comparison we give the time autocorrelation function at $T=18.15$ K for the same $N=256$ distribution, showing the normal rapid decay to zero [Fig. 10(b)]. The energy where $\Gamma_N(t)$ stops showing long-term correlations also depends on the initial conditions, but we find that the patterned behavior always disappears at ~ 16 K, and in most cases at even lower temperatures, indicating that not all the (distorted) tori vanish at the same energy.

In Figs. 11(a), 11(b), 11(c), and 11(d) we present our results for the energies -1.394, -1.165, -0.939, -0.792×10^{-14} ergs/atom, corresponding to the temperatures $T=18.15$, 28.44, 30.65, 36.71 K. In these pictures the distributions $g_{N_i}(\lambda)d\lambda$ (or the number of times λ was found in a bin of size 2.5×10^{-4} bits per 10^{-14} s for trajectories of length N_i) are plotted for $N_i=\{256,512,\ldots,8192\}$; the Lyapunov exponents are given in bits per 10^{-14} s. The area under each curve is proportional to the number of sample intervals for that curve and the area under the curve $N_i=256$ is 1. The reason for using this normalization is mainly graphical (this way of plotting gives all the results at a glance), but also the scaling reflects the fact that in reality we have two times more data for the distribution g_{N_i} than for the distribution $g_{N_{i+1}}$.

We immediately see that the distributions for $T=18.15$ K and $T=28.44$ K are unimodal for any N_i, while for $T=30.65$ K there are two peaks for $N_i=256$, 512, and 1024, and for $T=36.71$ K there are two well-defined peaks only for $N_i=256$. A comparison with Fig.

TABLE II. Standard deviation of λ at $T=18.15$, 28.44, 30.65, and 36.71 K, for $N=128$, 256, 512, 1024, 2048, 4096, and 8192. The units are bits per 10^{-14} s.

N \ T	18.15	28.44	30.65	36.71
128	5.77×10^{-3}	5.57×10^{-3}	6.61×10^{-3}	6.62×10^{-3}
256	1.75×10^{-3}	3.73×10^{-3}	4.40×10^{-3}	4.21×10^{-3}
512	1.69×10^{-3}	2.33×10^{-3}	3.16×10^{-3}	2.87×10^{-3}
1024	1.03×10^{-3}	1.74×10^{-3}	2.69×10^{-3}	2.41×10^{-3}
2048	8.21×10^{-4}	1.31×10^{-3}	2.21×10^{-3}	1.92×10^{-3}
4096	6.78×10^{-4}	9.56×10^{-4}	1.67×10^{-3}	1.50×10^{-3}
8192	5.29×10^{-4}	6.86×10^{-4}	1.25×10^{-3}	1.17×10^{-3}

7 shows that these results are consistent with this interpretation: for T close to the transition region the cluster exploring pathways over the three saddles around the minimum on the potential surface on short-time scales "sees" the phase space separating into two regions. One is a highly chaotic region with high kinetic energy (the motion in the well) and a much less chaotic region with high potential energy (the motion around the saddle).

This interpretation is confirmed by the fact that both
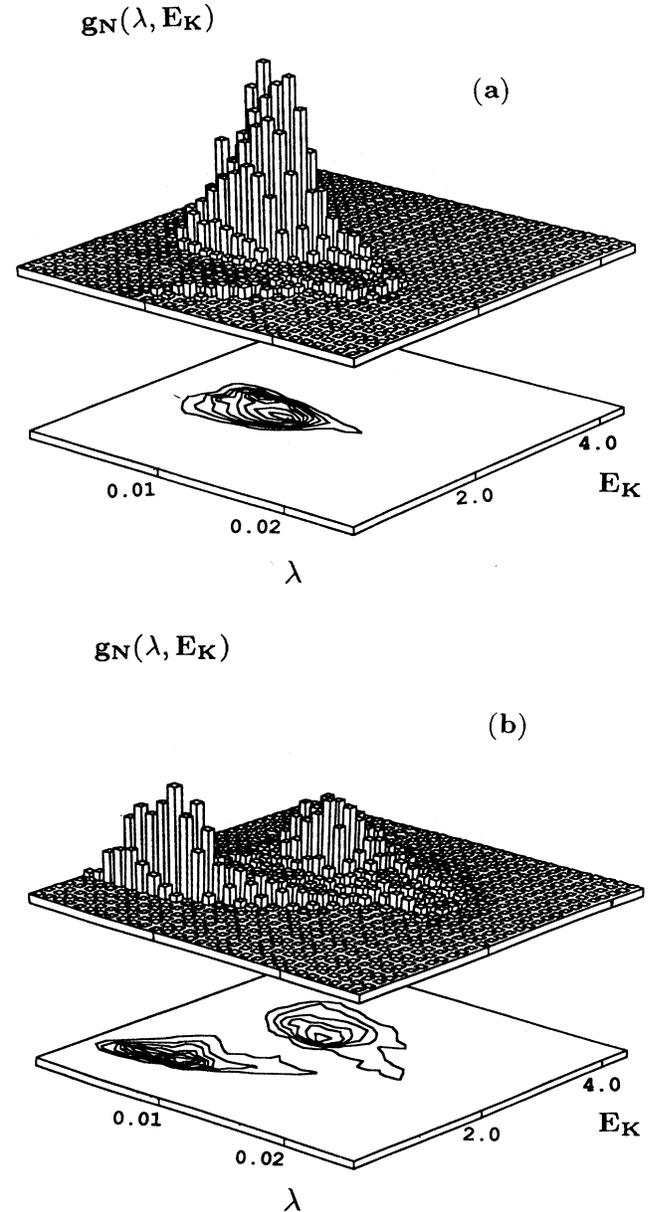
FIG. 12. $g_N(\lambda)$ vs λ, E_k at (a) $T=28.44$ K and at (b) $T=30.65$ K for $N=256$. The volume under the surface is normalized to unity. The units for λ are bits per 10^{-14} s. The units for E_K are 10^{-15} erg. Notice that the low-energy peak in (b) clearly develops out of the ridge visible on the bottom right of (a).

at $T=30.65$ K and $T=36.71$ K the Lyapunov exponent distribution strongly correlates with the distribution of the short-term averages of kinetic energies: an example is given in Fig. 12, where we can see g_{N_i} as a function of both λ, the largest local Lyapunov exponent, as well as $\langle E_{kin}(N_i) \rangle$, the short-term average kinetic energy, for $T=30.65$ K, $N_i=256$ [Fig. 12(b)], and contrast it with $T=28.44$ K, $N_i=256$ [Fig. 12(a)]. Of course Fig. 11 (or Fig. 12) also gives an estimate of the relative importance of the two regions. Moreover we can see that while for $T=30.65$ K the separation of trajectories into trajectories that move in the high-chaos region and trajectories that move in the low-chaos region is meaningful up to trajectories of length $N_i=1024$, at $T=36.71$ K trajectories of length $N=512$ already overlap both regions.

Table I gives the average of the distribution for each value N_i at the various temperatures. Whatever the temperature, λ shifts toward lower values with increasing N, implying that the asymptotic value for the largest Lyapunov exponent can only be obtained with trajectories of more than 10^4 steps.

Similarly, Table II gives the standard deviation of the distribution for each value N_i at the various temperatures. Abarbanel, Brown, and Kennel [7] convincingly argue that for predictive purposes this is the quantity

that really matters, since broad distributions, even without explicit bimodality, imply different rates of growth of small perturbations in the evolution of the system in different parts of the phase space and the presence of "critical" regions of rapid changes. Of course in this case the critical region is precisely identified by the existence of a second maximum in the distributions, and has been seen to correspond to the motion in the potential well. More detailed attempts to classify the regions for the generic argon cluster can be found in Refs. [8] and [23].

Since in the limit $N \to \infty$ the local Lyapunov exponents converge to the Lyapunov exponents, we expect the standard deviation σ to go to zero as $N \to \infty$. In Ref. [7] a scaling exponent ν has been defined by $\sigma(N) \sim N^{-\nu}$, and we find that for temperatures in the range $T \in [18, 37]$ and for our set of N_i values $\nu \simeq 0.8$–0.9, confirming previous results [7]; however, our estimate of ν still shows a systematic trend towards lower values at higher N, and we do not judge it to have reached the asymptotic value.

A better way to look at the dependence on N on the entire range of the distribution requires us to go back and review our definition of local Lyapunov exponents. If $d(N)$ is the (infinitesimal) distance between two trajectories at time N, we define λ_N implicitly by the relation
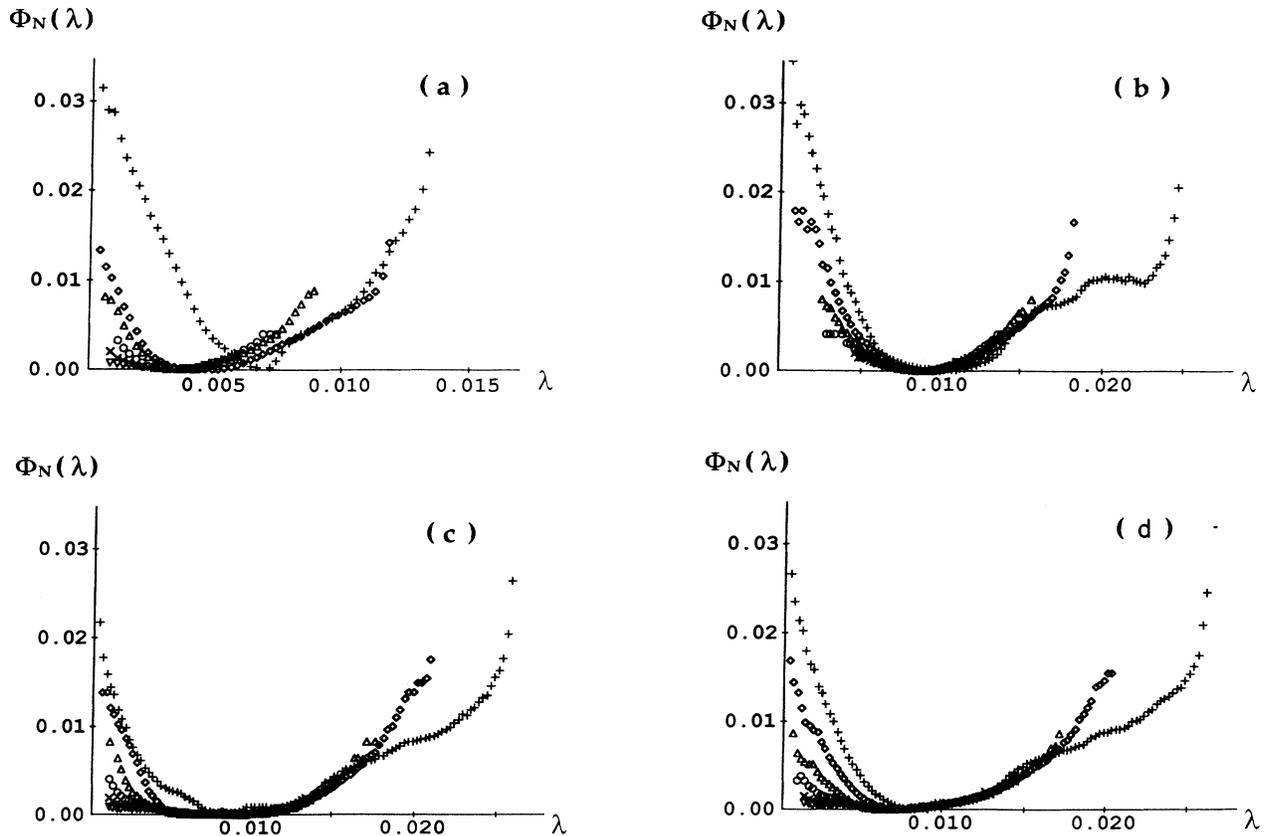
FIG. 13. $\Phi_n(\lambda)$ [Eq. (9)] vs λ at (a) $T=18.15$ K, (b) $T=28.44$ K, (c) $T=30.65$ K, (d) $T=36.71$ K, for $N=256$ (+), $N=512$ ($\Diamond$), $N=1024$ ($\triangle$), $N=2048$ ($\bigcirc$), $N=4096$ ($\times$), $N=8192$ (∇).

$$\mu(N) \equiv \frac{d(N)}{d(0)} \sim e^{N\lambda_N} .$$ (7)

A more precise definition is [6]

$$\mu(N) \equiv \frac{d(N)}{d(0)} \sim N^{\gamma_N} e^{N\lambda'_N} .$$ (8)

The difference between λ_N and λ'_N becomes meaningful only if the local Lyapunov exponent is very small when computed from sample intervals of many time steps, as happens when the orbit is close to a regular region, because then the divergence of nearby points is described by the algebraic exponent γ_N.

These two kinds of behavior can be efficiently distinguished by noting that if the power-law corrections are not important, then the probability distribution $P(\lambda_N; N)$ of sample Lyapunov exponents scales with N as $P(\lambda_N; N) \sim e^{-N\Phi(\lambda)}$ for $N \to \infty$; the asymptotic function $\Phi(\lambda)$ is known as the *spectrum* of effective Lyapunov exponents [24]. In general $\Phi(\lambda)$ has a minimum ($=0$) at $\lambda = \bar{\lambda}'$ and is positive and finite for $\lambda \le \lambda_{max}$, where λ_{max} is the Lyapunov exponent of the most unstable periodic orbit. From our distributions we can easily derive the finite-N approximation [6]

$$\Phi_N(\lambda) = \frac{1}{N} \ln \frac{P(\lambda_N; N)}{P_{max}(N)} .$$ (9)

Plots of this quantity as a function of λ at $N_i = \{256, 512, \ldots, 8192\}$ for the various medium-high energies considered before are presented in Fig. 13. (Remember that to get a meaningful result the power-law

behavior should be just a correction on the dominant exponential trend.) We see that for all these energies the plots at different N_i present a certain degree of data collapse. In fact, if we exclude the points belonging to the curve $N = 256$, starting from the right of the figures we can clearly distinguish a region where there is pure exponential scaling law at medium-large values of λ, and then a region where the power-law exponent has stronger

(a)

(b)

FIG. 15. (a) Minima for Ar_7; (b) schematic view of the local minima and transition states.
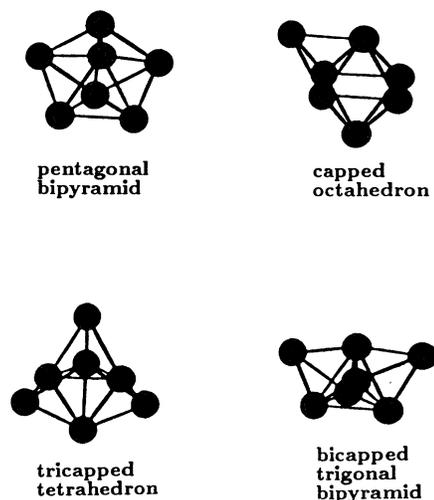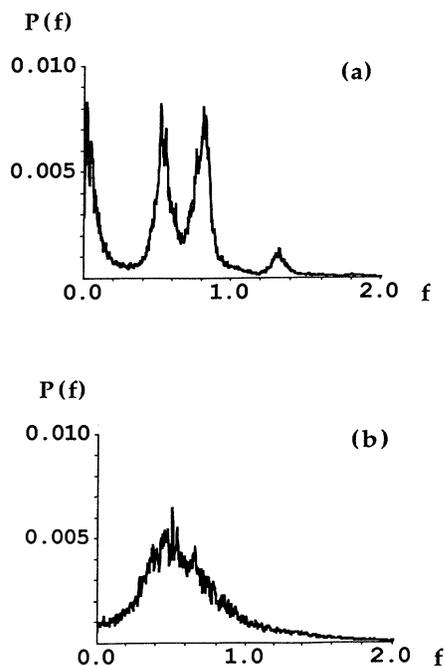
FIG. 14. Power spectra calculated separately for the two kinds of motion of $T = 30.65$ K: (a) regular and (b) chaotic. The frequency is in 10^{12} s^{-1}.

and stronger influence towards smaller and smaller values of λ.

This kind of separation is what led Sepúlveda, Badii, and Pollak [6] to try to divide the power spectrum in a portion that came from the regular regions and a portion that came from chaotic regions. In fact, we use the data from Fig. 12(b), which correlates local kinetic energy and

local Lyapunov exponents for a cluster at $T = 30.65$, $E = -0.939 \times 10^{-14}$ ergs/atom, to separately get the power spectrum of the low-chaos–low-kinetic-energy motion over the saddle, and the power spectrum of the high-chaos–high-kinetic-energy motion in the potential well (Fig. 14). Such a decomposition for Ar_3 was attempted before [9] on the basis of the distributions for the
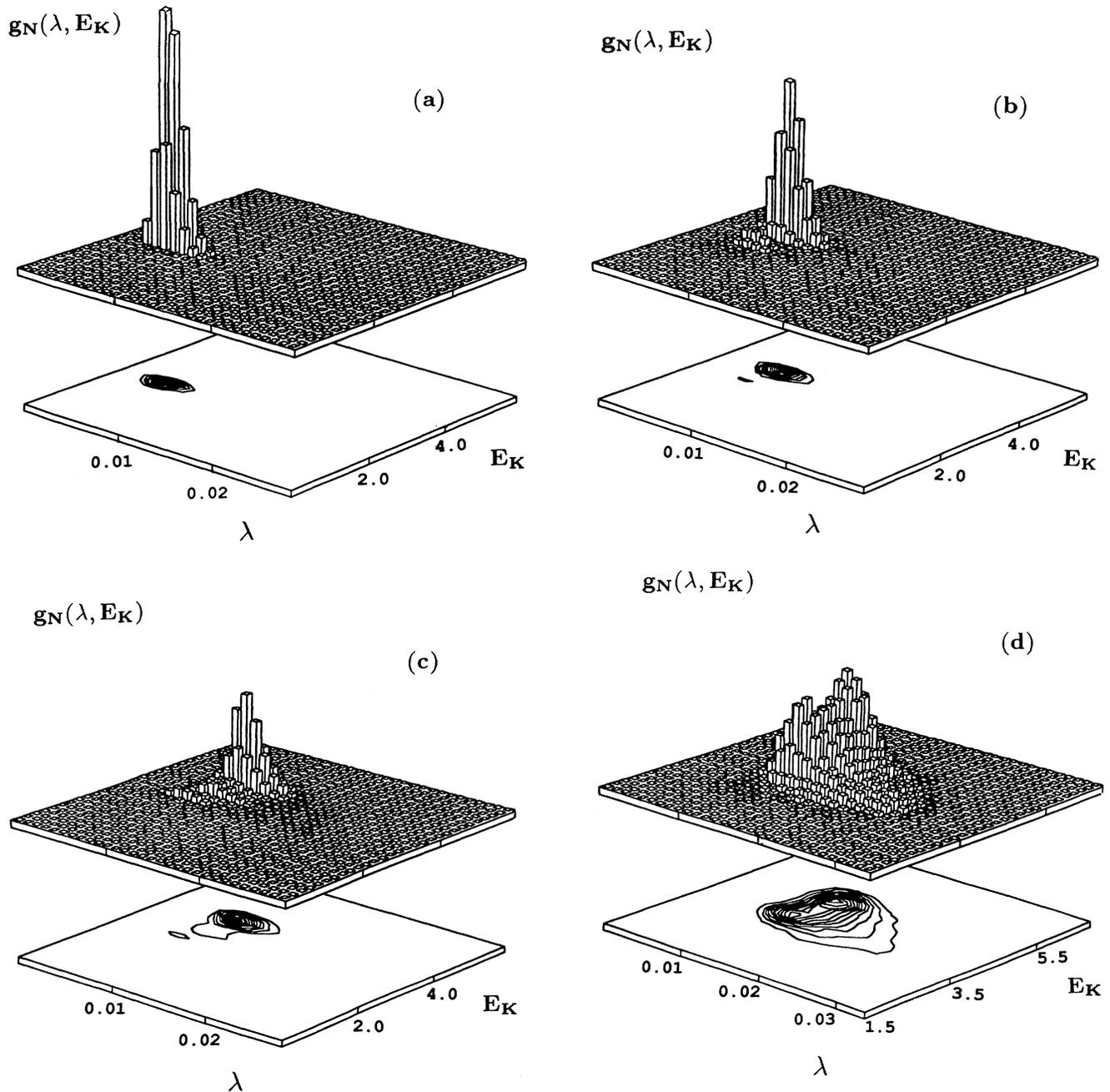
FIG. 16. $g_N(\lambda, E_K)$ vs λ, E_K for Ar_7, $N = 256$ at (a) $E = -0.355$, (b) $E = -0.341$, (c) $E = -0.328$, (d) $E = -0.300$, (e) $E = -0.280$, and (f) $E = -0.265 \times 10^{-13}$ ergs/atom. The volume under the surface is normalized to $\frac{1}{4}$ for (a), (b), and (c) and to 1 for (d), (e), and (f). The units for λ are bits per 10^{-14} s. The units for E_K are 10^{-15} ergs.

$g_N(\lambda, E_K)$

$g_N(\lambda, E_K)$

(f)

(e)
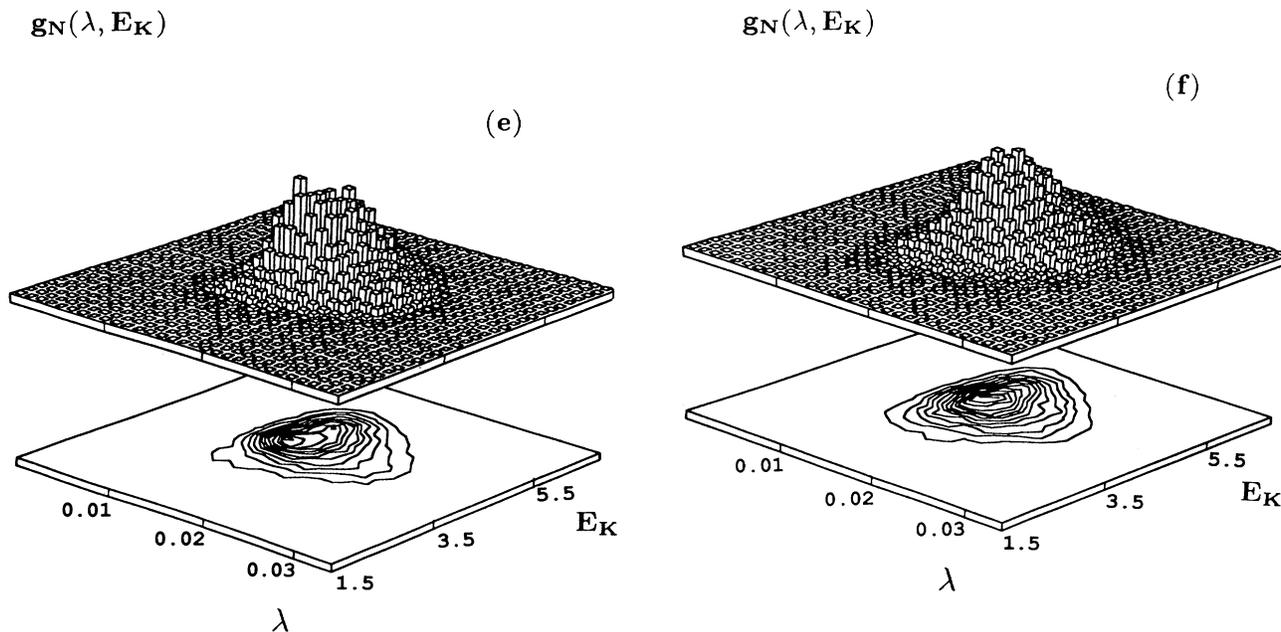
FIG. 16. *(Continued)*.

local kinetic energy only, and succeeded because, as we can see from Fig. 12, the projection on the $\langle E_K \rangle$ axis gives quite separated peaks too.

C. Ar$_7$ cluster

In contrast with Ar$_3$, Ar$_7$ has a fairly complicated potential surface, with four distinct local minima corresponding to four nonequivalent stable configurations; Figs. 15(a) and 15(b) show a schematic view of the local minima and transition states for this system, from which we can see that the topology of the network of minima and saddles connecting them is indeed much more involved than in the previous case. Wales and Berry [12] examined this structure in detail, and by short-term averaging the kinetic energy of the cluster [9] were able to separate the motion through the saddles from the motion in the potential wells. This task we can perform in a much more pictorial way by looking at the joint distributions of local Lyapunov exponents and local kinetic energy: the succession of energies in Fig. 16, $E = -0.355$, (a), $E = -0.341$ (b), $E = -0.328$ (c), $E = -0.300$ (d), $E = -0.280$ (e), and $E = -0.265 \times 10^{-13}$ ergs/atom (f) shows very directly how the motion, first confined in the deeper potential well, the pentagonal bipyramid structure (a), starts seeing a second minimum, the capped octahedron (b), and then a third one, the tricapped tetrahedron (c), and how high the energy should be raised before the cluster becomes able to flow quickly from one structure to another (f).

As is clearly explained in Ref. [12] the multimodality is observable because the saddle crossing is a relatively infrequent event at the total energy in question, and the short-term average kinetic energy for the various minima are very different. We do not really observe multimodali-

ty in the Lyapunov distributions, but the very fact that they are so spread out is already enough to alert us about the presence of regions in phase space that contribute very differently to the chaotic properties of the cluster. As for Ar$_3$, if we plot the distributions for various N_i, at a certain point we observe the disappearance of multimodality, and are able to define a time scale at which the system is completely ergodic.

The apparent discrepancy between the energies in Fig. 16 and the saddle points in Fig. 15 is due to the fact that for a cluster of this size, the total energy the cluster must have in order to go over a saddle in an observable time is roughly a factor of 2 greater than the barrier height. Therefore a cluster with an energy of -0.355×10^{-13} ergs/atom is still basically confined in the pentagonal bipyramid structure, its lowest minimum. But what happens at still lower energies? At $E = -0.372 \times 10^{-13}$ ergs/atom we were able to isolate three different behaviors: (i) basically ergodic behavior in the pentagonal bipyramid [Fig. 17(a)]; (ii) basically ergodic behavior in the capped octahedron well (if we put it there it does not have enough energy to cross back) [Fig. 17(b)]; and (iii) regular in the pentagonal bipyramid structure. Therefore, even with so many degree of freedom, and at a relatively large energy, regular motion can persist for a very long time.

We also performed the power spectrum analysis for Ar$_7$ at $E = -0.328 \times 10^{-13}$ ergs/atom, decomposing the total power spectrum in portions generated by the motion around the three lowest potential minima by using the data from Fig. 16(c); Fig. 18 shows the results for the three peaks identifiable in that picture, and again the trend seems to be that the more regular motion is responsible for the narrow features while the chaotic part gives the background.

IV. DISCUSSION

At this point we can examine the results and draw conclusions. First, let us review what we find for any system at low total energy. In that situation the distributions of local Lyapunov exponents are characterized by three features: (i) they present spikes; (ii) they do not show a smooth convergence with increasing N, the length of the averaging interval; and (iii) they strongly depend on the initial conditions. A careful analysis shows that distributions that present these characteristics correspond to totally nonergodic dynamics, where the motion is confined to (possibly strongly distorted) tori. The apparent para-

dox of having $\lambda_{max} > 0$ with regular motion is solved by considering the limit $\tau \to 0$, i.e., by sending the time step for the integration of the equation of motion to zero. In such a process we see that λ_{max} does indeed decrease linearly with τ, and can be then extrapolated to be zero at $\tau = 0$ as it should. In contrast, for a really chaotic regime λ_{max} stays constant when we decrease τ. However, different initial conditions give different slopes for the linear dependence of λ_{max} on τ, showing that various trajectories meet various amounts of potentially chaotic "disturbances"; we find in fact that for any τ the distributions are still well defined, can be definitively associated with the initial conditions, and give an idea of what percentage of the trajectory is spent in proximity of chaotic regions.

Depending on the initial conditions, at slightly higher values of the total energy, the motion can be regular or chaotic; the distributions corresponding to regular motions have the same characteristics as before, but for initial conditions in the chaotic regions the spikes disap-
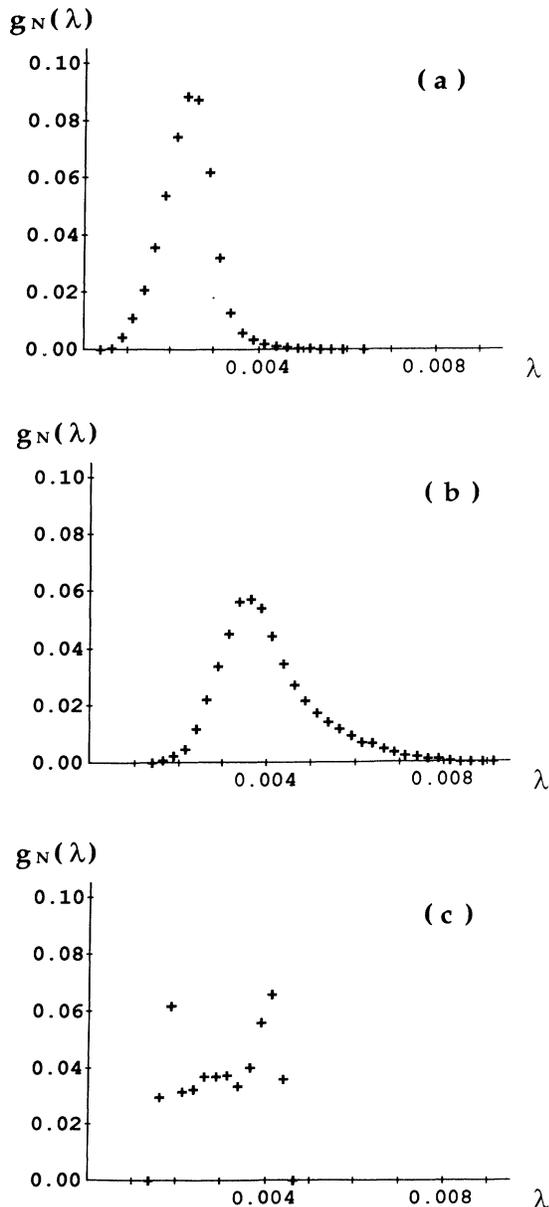
FIG. 17. $g_N(\lambda)$ vs λ for Ar$_7$ at $E = -0.372 \times 10^{-13}$ ergs/atom, $N = 256$, for three different initial conditions.
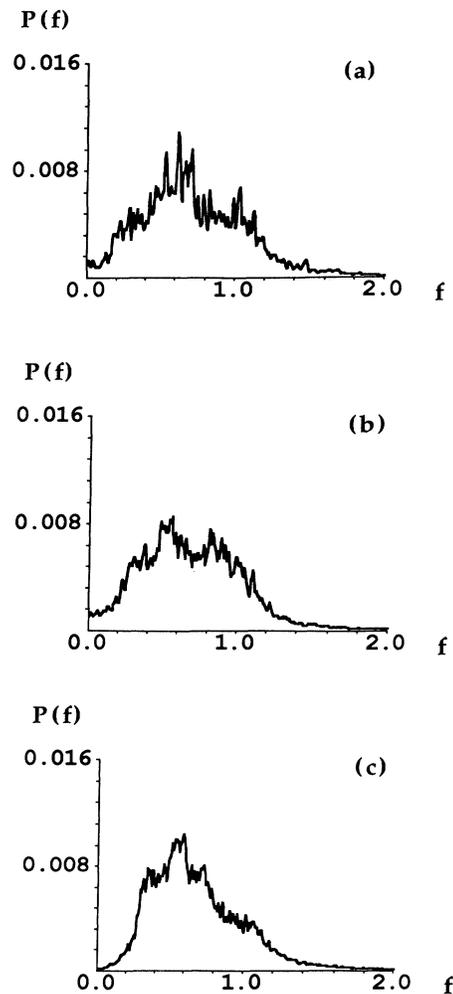
FIG. 18. Power spectra calculated separately for the motion in the three lowest wells at $E = -0.328 \times 10^{-13}$ ergs/atom. The frequency is in 10^{12} s^{-1}.

pear [see Figs. 5(a) and 6(a)]. Nevertheless the distributions still do not converge smoothly with N, as they would if the accessible phase space were characterized by a unique global Lyapunov exponent, which we were slowly approaching. But in this interval of energy values even when λ_{max} is definitively greater than zero there is another piece of evidence that also prevents us from diagnosing the situation as fully developed chaos: the power spectrum still consists of very narrow peaks, as though the lines characterizing the very low-energy systems had simply acquired a "thickness" without yet merging in a continuous spectrum (for an example from Ar$_3$, see Ref. [9]; our data for Hénon-Heiles look very similar to this); the information that we derive from the distributions of local Lyapunov exponents is therefore consistent with the power spectrum analysis.

For the Hénon-Heiles model the energy range for this regime is approximately $\frac{1}{8} \leq E \leq \frac{1}{6}$, where a random initial condition has a considerable probability of being in the chaotic region, but the probability of escaping is practically zero; but since one cannot raise the energy any further without increasing the latter, in this model you can never see what happens next. However, for Ar$_3$ this situation corresponds to temperatures between ~ 10 and 18 K, well below the dissociation temperature, and there is thus ample room for further investigations. We find that for intermediate-high values of the energy, $-1.4 < E < -1.0 \times 10^{-14}$ ergs/atom or $18 < T < 30$ K, the distributions of short-term Lyapunov exponents are smooth, almost Gaussian, curves with no dependence from the initial conditions, and show a reasonable convergence with increasing N [Figs. 11(a) and 11(b)]. Therefore the system is fully ergodic and the accessible phase space is characterizable by a single Lyapunov exponent. In this range the dynamics look completely chaotic and the power spectra have nonzero components in a large band of frequencies [9].

But at still higher energies a new effect shows up in the distributions: now the energy is high enough to allow saddle crossings, and this process leaves a signature on the shortest N distributions in the form of bimodality [Figs. 11(c) and 11(d)]. In fact the motion in the saddle region has a lower average value of λ_{max} and happens on time scales comparable with the lowest N values presented here. Hinde, Berry, and Wales [23] have shown how the decrease in local K entropy (the sum of positive Lyapunov exponents) in the saddle region is associated with the "funnelling" of trajectories due to the shape of the potential energy surface; the relation between the

shape of the saddle and the local ordering effect for different argon clusters has also been studied in great detail [25]. However, our distributions not only give an immediate hint that a new dynamical process is happening but also reveal the time scale associated with it. The double classification in average short-term kinetic energy and local largest Lyapunov exponent (Fig. 12) allows then a very precise separation of the motion in the potential well from the motion over the saddle, which we have exploited to get the contribution to the power spectrum from the different regions of the potential surface.

Our results for Ar$_7$ show that these ideas can be successfully used even to study more complicated situations. Here through the distributions we are able to identify regular behavior in the potential minimum, ergodic behavior in the various potential wells, and saddle crossings in the appropriate energy ranges. Even though the topology of the potential surface is now much more involved, the distributions $g_N(\lambda, E_K)$ allow a good reconstruction of the dynamical processes at the various energies, with an estimate both of the time characteristically spent in each potential minimum and the time for crossing from one to another.

Our conclusion is therefore that the operation of measuring the Lyapunov exponent can give much more than a single estimate characterizing the system globally, and furthermore that sometimes the global characterization itself may be misleading. The usual technique to calculate Lyapunov exponents requires one to consider plots of λ versus a number of integration steps, to discard the transient portion and to concentration on the asymptotic behavior: but our claim is that the "junk" at the beginning of those plots, before they converge to nice stable values, can give a great deal of additional information on the dynamics of the system, and is in fact much more interesting than the limiting values [25]. In particular our results show how a study of the *sample distributions* of Lyapunov exponents, as they evolve from local to global, gives insight into how ergodicity evolves in time.

ACKNOWLEDGMENTS

[1] V. I. Oseledec, Trans. Mosc. Math. Soc. **19**, 197 (1968).

[2] G. Benettin, L. Galgani, and J.-M. Strelcyn, Phys. Rev. A **14**, 2338 (1976).

[3] G. Benettin, L. Galgani, A. Giorgilli, and J.-M. Strelcyn, Meccanica **15**, 9 (1980).

[4] J.-P. Eckmann and D. Ruelle, Rev. Mod. Phys. **57**, 617 (1985).

[5] R. Kosloff and S. A. Rice, J. Chem. Phys. **74**, 1947 (1981).

[6] M. A. Sepúlveda, R. Badii, and E. Pollak, Phys. Rev. Lett.

63, 1226 (1989).

[7] H. D. I. Abarbanel, R. Brown, and M. B. Kennel, J. Nonlinear Sci. **1**, 175 (1991).

[8] D. J. Wales and R. S. Berry, J. Phys. B **24**, L351 (1991).

[9] T. L. Beck, D. M. Leitner, and R. S. Berry, J. Chem. Phys. **89**, 1681 (1988).

[10] C. Amitrano and R. S. Berry, Phys. Rev. Lett. **68**, 729 (1992).

[11] D. M. Leitner, R. S. Berry, and R. M. Whitnell, J. Chem.

Phys. **91**, 3470 (1989).

[12] D. J. Wales and R. S. Berry, J. Chem. Phys. **92**, 4283 (1990).

[13] M. Hénon and C. Heiles, Astron. J. **69**, 73 (1964).

[14] M. C. Gutzwiller, *Chaos in Classical and Quantum Mechanics* (Springer-Verlag, New York, 1990).

[15] A. J. Lichtenberg and M. A. Lieberman, *Regular and Stochastic Motion* (Springer-Verlag, New York, 1983).

[16] L. Verlet, Phys. Rev. **159**, 98 (1967).

[17] D. W. Heermann, *Computer Simulation Methods* (Springer-Verlag, Berlin, 1986).

[18] P. Grassberger and I. Procaccia, Physica **13D**, 34 (1984).

[19] Y. B. Pesin, Russ. Math. Surveys **32(4)**, 55 (1977).

[20] A. Wolf, J. B. Swift, H. L. Swinney, and J. A. Vastano, Physica **16D**, 285 (1985).

[21] M. Casartelli, Nuovo Cimento B **76**, 97 (1983).

[22] M. C. Carotta, C. Ferrario, G. Lo Vecchio, and L. Galgani, Phys. Rev. A **17**, 786 (1978).

[23] R. J. Hinde, R. S. Berry, and D. J. Wales, J. Chem. Phys. **96**, 1376 (1992).

[24] P. Grassberger, R. Badii, and A. Politi, J. Stat. Phys. **51**, 135 (1988).

[25] R. J. Hinde and R. S. Berry, J. Chem. Phys. (to be published).